IEEE Access
Multidisciplinary | Rapid Review | Open Access Journal

SPECIAL SECTION ON HUMAN-DRIVEN EDGE COMPUTING (HEC)

Received March 1, 2020, accepted March 13, 2020, date of publication March 18, 2020, date of current version March 27, 2020.

Digital Object Identifier 10.1109/ACCESS.2020.2981463

Cooperative Autonomous Driving Oriented MEC-Aided 5G-V2X: Prototype System Design, Field Tests and AI-Based Optimization Tools

HUISHENG MA[1], (Member, IEEE), SHUFANG LI[1], (Senior Member, IEEE), ERQING ZHANG[1], ZHENGNAN LV[2], JING HU[2], AND XINLEI WEI[3]

[1]School of Information and Communication Engineering, Beijing University of Posts and Telecommunications, Beijing 100876, China
[2]Potevio Information Technology Company Ltd., Beijing 100080, China
[3]Research Institute of Highway Ministry of Transport, Beijing 100088, China

Corresponding author: Huisheng Ma (mhs@bupt.edu.cn)

This work was supported in part by the National Key Research and Development Program of China under Grant 2019YFB2102300, in part by the Breeding Project for New Generation AI of Beijing under Grant Z181100008918008, and in part by the National Science and Technology Major Project of China under Grant 2016ZX03001024.

ABSTRACT Vehicle-to-Everything (V2X) requirements from cooperative autonomous driving can be characterized as ultra-reliable, low latency, high traffic, and high mobility. These requirements introduce great challenges in the air interface and protocol stack design, resource allocation, network deployment, and all the way up to mobile (or multi-access) edge computing (MEC), cloud and application layer. In this paper, we present a cooperative autonomous driving oriented MEC-aided 5G-V2X prototype system design and the rationale behind the design choices. The prototype system is developed based on a next-generation radio access network (NG-RAN) experimental platform, a cooperative driving vehicle platoon, and an MEC server providing high definition (HD) 3D dynamic map service. Field tests are conducted and the results demonstrate that the combination of 5G-V2X, MEC and cooperative autonomous driving can be pretty powerful. Considering the remaining challenges in the commercial deployment of 5G-V2X networks and future researches, we propose two artificial intelligence (AI) based optimization tools. The first is a deep-learning-based tool called deep spatio-temporal residual networks with a permutation operator (PST-ResNet). By providing city-wide user and network traffic prediction, PST-ResNet can help to reduce the capital expense (CAPEX) and operating expense (OPEX) costs of commercial 5G-V2X networks. The second is a swarm intelligence based optimization tool called subpopulation collaboration based dynamic self-adaption cuckoo Search (SC-DSCS), which can be widely used to solve complex optimization problems in future researches. The effectiveness of proposed optimization tools is verified by real-world data and benchmark functions.

INDEX TERMS V2X, MEC, field tests, deep learning, swarm intelligence, cuckoo search.

I. INTRODUCTION

Vehicle-to-Everything (V2X) communications have drawn great attention in both industrial and academic fields for more than ten years. The V2X applications in the 3GPP specification contain the following four different types (see Fig.1): vehicle-to-vehicle (V2V), Vehicle-to-Infrastructure (V2I), vehicle-to-network (V2N), and vehicle-to-pedestrian (V2P) [1]. Today, there are two key classes of radio access technologies (RATs) enabling V2X communications, which are standardized respectively in 3GPP and IEEE. The V2X from 3GPP is called Cellular-V2X (C-V2X), including LTE-V2X, LTE-eV2X, and 5G-V2X (NR-V2X). While IEEE 802.-11p and its evolution version 802.11bd are the foundation of V2X systems such as dedicated short range communications (DSRC) in the U.S. and cooperative intelligent transport systems (C-ITS) in Europe. V2X systems based on IEEE 802.11p have similar communication types.

The associate editor coordinating the review of this manuscript and approving it for publication was Rongbo Zhu.

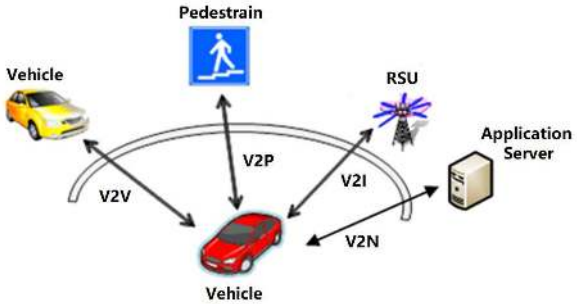

FIGURE 1. Types of V2X applications defined in 3GPP.

The Multi-hop communication type is supported in some IEEE 802.11p V2X systems, such as C-ITS, which lead to the research area of routing in Vehicular Ad-hoc Network (VANET) [2], [3].

There has been tremendous interest in the development of vehicles capable of autonomous driving, from both the research community and industry. In 2014, the SAE organization published the J3016 standard [4], which aims at providing a common terminology and classification levels for autonomous driving. Five levels of autonomous driving are defined according to their relative extent of automation, ranging from level 1: Driver Assistance to level 5: Full Automation. In the past two years, several Level 4 (High Automation) autonomous driving vehicles and applications have been developed, of which the most typical one is ''Waymo One''. Most autonomous vehicles currently in development depend on a perception subsystem consisting of onboard sensors of the vehicle itself. Although this self-only method has already been demonstrated in field tests, it presents some drawbacks: the limited perception range of onboard sensors and lack of collaborative maneuvers with related vehicles.

The combination of V2X and autonomous driving enables the creation of cooperative autonomous driving, which has two key cooperative features: sensing and maneuvering. Based on these features, cooperative autonomous driving allows vehicles to exchange information gathered from local sensors and permits inter-vehicle coordination of maneuvers. The integration of onboard sensors and V2X communication could also result in a solution that is more cost-effective than an approach based on high-quality sensors only [5]. Thus, we should set the target that the combination of V2X and autonomous driving is to greatly improve the traffic safety, efficiency, driver comfort and cost performance of autonomous driving vehicles.

To achieve this target, cooperative autonomous driving needs to impose stringent latency, reliability, throughput and mobility requirements on the V2X system. Studies indicate that both LTE-V2X/eV2X and IEEE 802.11p can reliably support safety applications that demand an end-to-end latency of around 100 milliseconds as long as the vehicular density is not very high but fall short of supporting more stringent communication requirements of many advanced vehicular

TABLE 1. QoS requirements of advanced V2X applications supported by 5G-V2X.

Application scenarios	Max end-to-end latency (ms)	Reliability (%)	Data rate (Mbps)
Vehicle Platooning	10 - 500	90 - 99.99	50 - 65
Advanced Driving	3 - 100	90 - 99.999	10 - 50
Extended Sensors	3 - 100	90 - 90.999	10 -1000
Remote Driving	5	99.999	UL:25, DL:1

applications, which are believed to be critical in enabling fully autonomous vehicles [6]. NR-V2X and IEEE 802.11bd now being in the standardization process are expected to diminish the performance gap. For example, NR-V2X are designed to provide an end-to-end latency of 3ms and high reliability up to 99.999% [7] and support the advanced V2X applications categorized into four groups: vehicle platooning, advanced driving, extended sensors, and remote driving [8]. The quality of service (QoS) requirements of these applications defined by 3GPP are summarized in Table 1.

In this paper, we present a prototype system design and field tests for cooperative autonomous driving oriented V2X. As introduced in our previous work [9], the development of this prototype system is a part of an ongoing research project named ''The Research and Demonstration of 5G Key Technology Oriented Autonomous Driving'', which is funded by National Science and Technology Major Project of China. The QoS requirements are to achieve as low as 1ms delay between user planes of air interface, 99.999% air interface reliability through retransmissions limited in 10ms duration, at least 2000 vehicles per kilometer for low speed, 200 vehicles per kilometer for high speed, 50Mbps cell edge throughput for V2I, and 10Mbps rate for V2V.

Comparing with Table 1, it can be seen that the ultra-reliable low latency (URLLC) requirement of this V2X prototype system is more stringent than NR-V2X. Since NR-V2X standardization starting in 3GPP Release 16 has not yet been completed, our work can be regarded as a proof of concept prior to the commercial development of 5G-V2X based cooperative autonomous driving. To the best of the authors' knowledge, only a few field tests integrate 5G-V2X and autonomous driving. Field trial activities focus on the V2V latency of an NR-V2X prototype system applying to truck platooning are presented in [10]. An earlier field test for 5G-V2X enabling automated emergency braking is presented in [11].

Although the capability of 5G-V2X is proved to meet the requirements of cooperative autonomous driving through the development and test of our prototype system, we find that there are still some challenges in the development and deployment of commercial systems and the research of 5G-V2X evolution which have not been fully studied at present.

In our opinion, the first challenge is how to effectively reduce the CAPEX and OPEX costs in the commercial deployment and operation of 5G-V2X networks. The reason lies in that URLLC is considered to be the most critical

requirement for 5G-V2X, but it has to be meet at the cost of spectral efficiency [12]. Coping with the simultaneous high traffic requirement, it is necessary to implement the ultra-dense network (UDN) with multi-carrier aggregation for commercial 5G-V2X services, which brings high deployment and operational costs. During the solutions, more attention should be paid to the technique for precise user numbers and network traffic predicting. Because it is a key technique to reduce the costs, which can be used in base station deployment density and location optimization, minimizing the energy consumption by switching off under-utilized carriers and base stations, improve resource allocation efficiency and user experience and so on.

The second challenge is how to solve the increasingly complex optimization problems in the evolution of 5G-V2X. Multi-hop communication, cognitive radio, and other technologies should be considered to enhance network coverage and application scenarios, and improve the contradiction between low spectrum efficiency and insufficient spectrum resources. These technologies bring additional complex optimization problems in routing, resource allocation, interference management, etc. It is necessary to study some widely applicable tools for solving these complex optimization problems.

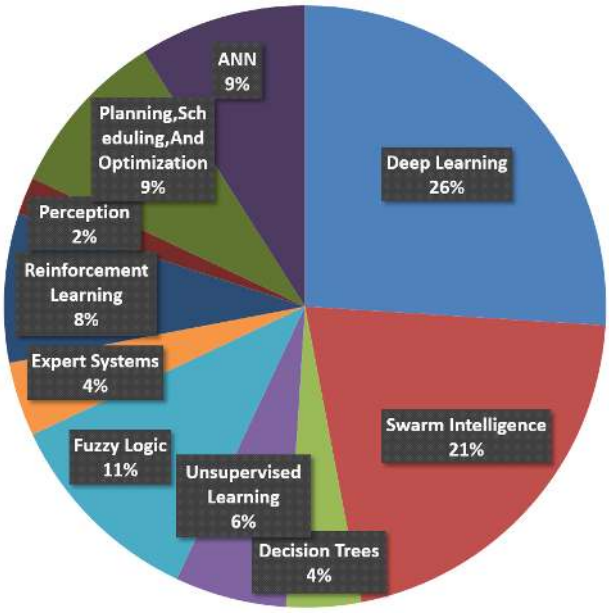

FIGURE 2. Percentage of AI techniques used in V2X applications according to [13].

Rapid progress in artificial intelligence (AI) techniques open up new opportunities to solve these challenges. AI has been used to address the complex and dynamic challenges of the V2X paradigm. In a survey of AI for V2X given by Tong *et al* in [13], Deep Learning and Swarm Intelligence are showed to be two popular and widely used AI techniques, occupying nearly half of the referenced 151 research articles (see Fig.2). The representative application fields of deep learning and swarm intelligence in V2X researches include the prediction of network and road traffic, resource allocation, congestion control, routing, and clustering, etc., which can be found in [14]–[21]. This paper also focuses on these two techniques. Accordingly, two AI-based optimization tools are proposed to solve the two challenges mentioned above, one related to Deep Learning, and the other related to Swarm Intelligence.

For the first challenge, we propose a deep-learning-based tool to optimize predictions based on unique properties of spatio-temporal data including vehicle trajectories and network traffic, which are called deep spatio-temporal residual networks with a permutation operator (PST-ResNet). The primary consideration is that energy reduction schemes like switching off under-utilized base stations need not only the spatio-tempral prediction result of a single cell but also each and every cell of the city-wide network. PST-ResNet is designed to employ convolution-based residual networks to model the nearby and distant spatial dependencies between any two regions in a city and the closeness, period, and trend properties of temporal dependencies, which is similar to the methodology adopted in ST-ResNet proposed by Junbo Zhang *et al* in [22]. The main improvement is that with permutation operation PST-ResNet can support irregular regions dividing including dividing by cell coverages, whereas ST-ResNet can only support grid-based regions dividing which should be regarded as a special case in PST-ResNet. Experiments on Beijing taxicabs' trajectories and meteorological data demonstrate that the proposed PST-ResNet outperforms ST-ResNet and several other well-known methods.

For the second challenge, we provide a widely applicable optimization tool based on Swarm Intelligence to solve complex optimization problems in the research of 5G-V2X and its evolution. This tool is called Subpopulation Collaboration based Dynamic Self-adaption Cuckoo Search (SC-DSCS). SC-DSCS is designed to improve the convergence rate and optimization precision of Cuckoo Search (CS), which is very effective in solving global optimization problems. The global convergence of CS has been proved using a Markov chain framework in [23]. Studies show that CS could outperform other Swarm Intelligence methods including Differential Evolution (DE), Simulated Annealing (SA), Particle Swarm Optimization (PSO), Genetic Algorithm (GA) and Artificial Bee Colony (ABC) [24]. In fact, DE, SA, and PSO are special cases of CS [25]. The applications of CS in V2X related researches have produced many achievements, mainly focusing on routing, spectrum allocation, clustering and other technical fields, some of which can be found in [19]–[21], [26]–[35]. In SC-DSCS, the population of cuckoos is divided into two subgroups, and a collaboration mechanism is introduced between the two groups to enhance the local search capability. Borrowing the idea of Grey Wolf Optimizer (GWO) that the alpha (best candidate solution), beta and delta have better knowledge about the potential location of prey [36], SC-DSCS creates an additional new bird's nest

based on the comprehensive assessment of the first three best bird's nests being found after each searching round. Nine benchmark functions are adopted to evaluate the performance of SC-DSCS. Simulation results show that SC-DSCS has better convergence speed and optimization precision than CS, ABC, DE, PSO, and RC-SSCS (an improved CS proposed in [37]).

A summary of the main contributions of this work are:

- Provide the design of a cooperative autonomous driving oriented 5G-V2X prototype system and conduct field tests to verify the promotion effect of 5G-V2X service on autonomous driving.
- Propose a deep-learning-based tool called PST-ResNet to optimize predictions based on spatio-temporal data including vehicle trajectories and network traffic, and demonstrate that PST-ResNet outperforms ST-ResNet and several other well-known methods by experiments on real-world data.
- Propose a widely applicable optimization tool called SC-DSCS based on Swarm Intelligence to solve complex optimization problems in the research of 5G-V2X and its evolution, and evaluate the performance of SC-DSCS and some other Swarm Intelligence methods adopting benchmark functions.

The remainder of the paper is organized as follows. Section II presents the design of the prototype system. Section III presents the field test process and results. Section IV describes the proposed deep-learning-based tool called PST-ResNet and the proposed widely applicable optimization tool called SC-DSCS based on Swarm Intelligence. Section V presents the evaluation results of PST-ResNet and SC-DSCS. Finally, we conclude and make a summary in section VI.

II. PROTOTYPE SYSTEM DESIGN

A. SYSTEM OVERVIEW

Our work is a part of "The Research and Demonstration of 5G Key Technology Oriented Autonomous Driving" project. We built a field test environment for cooperative autonomous driving oriented 5G-V2X communication using a 5G-V2X prototype system, an autonomous driving vehicle platoon and a mobile edge computing (MEC) server used as a map server providing high precision 3D map dynamic reconstruction service. According to the QoS requirements described in the introduction part, the 5G-V2X prototype system is designed and developed based on a next-generation radio access network (NG-RAN) experimental platform consisting network side devices including the core network (CN), baseband units (BBUs), remote radio units (RRUs) and antennas, and the user side devices i.e. user equipments (UEs). System frame structure, physical channels, network architecture and system procedure of the platform are modified to satisfy the stringent QoS requirements.

The autonomous driving vehicle platoon consists of five autonomous driving vehicles. Equipped with one UE, an autonomous driving vehicle supports sending environment perception information to the map server, receiving map update information from the server and broadcasting information to neighbors. The map server gives the over-the-horizon perception ability of the autonomous driving vehicle and plays an important role in the cooperation of vehicle and vehicle. Fig.3 illustrates the overall configuration for field tests of the prototype system with the view of applying 5G-V2X to cooperative autonomous driving.

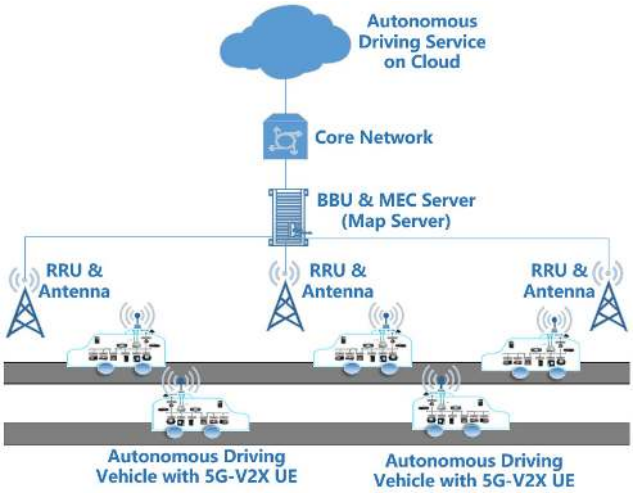

FIGURE 3. The overall configuration for field tests.

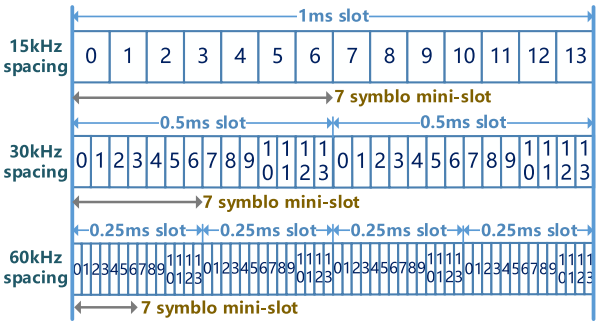

FIGURE 4. Using 60 kHz Subcarrier Spacing and 7 symbol mini-slot.

B. TECHNOLOGY PILLARS IN THE PROTOTYPE TO SATISFY STRINGENT QOS REQUIREMENTS

1) ULTRA RELIABLE AND LOW LATENCY DESIGN

In order to meet the low latency requirement of a one-time transmission delay (1ms) of the user plane (UP) for V2X communication, the short transmission-time-interval (TTI) design is the first technology being adopted. On the other hand, the use of higher sub-carrier spacing also facilitates latency reduction. Assuming one transmission block (TB) requires a fixed number of sub-carriers in a TTI, the length of TTI decreases as the sub-carrier spacing increases. Considering the flexible OFDM numerology introduced in 5G NR and the propagation characteristics of 3.5GHz band, 60 kHz sub-carrier spacing is used in the prototype system, the length of TTI is set to 7 symbols. The contrast effect of different sub-carrier spacing and TTI length can be found in Fig.4.

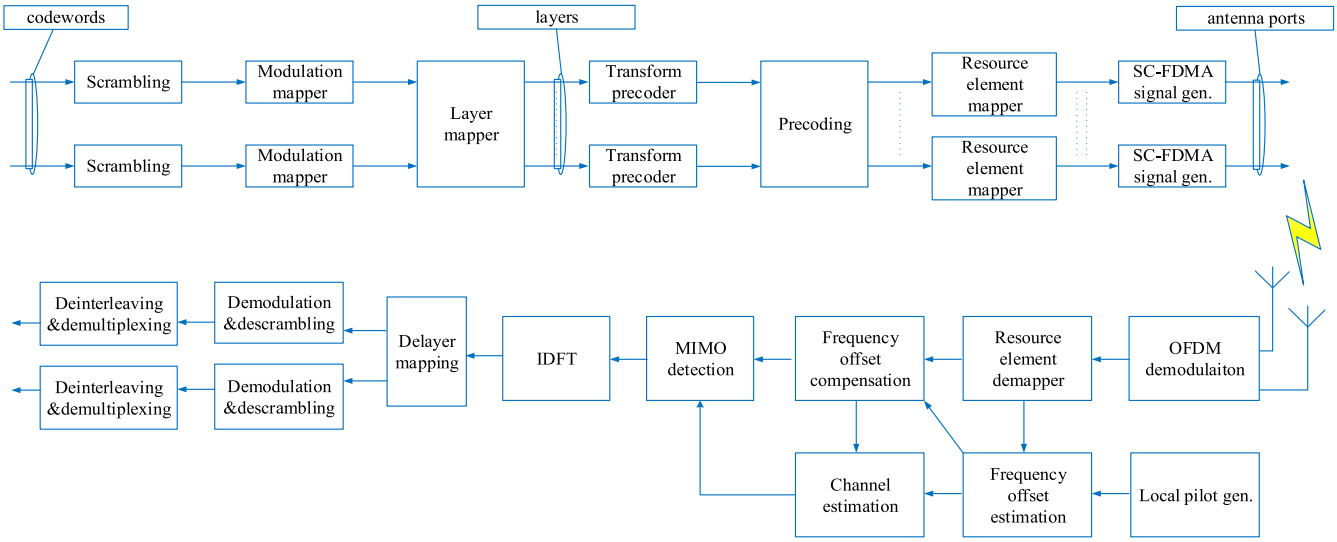

FIGURE 5. Overview of V2V physical channel processing in the prototype system.

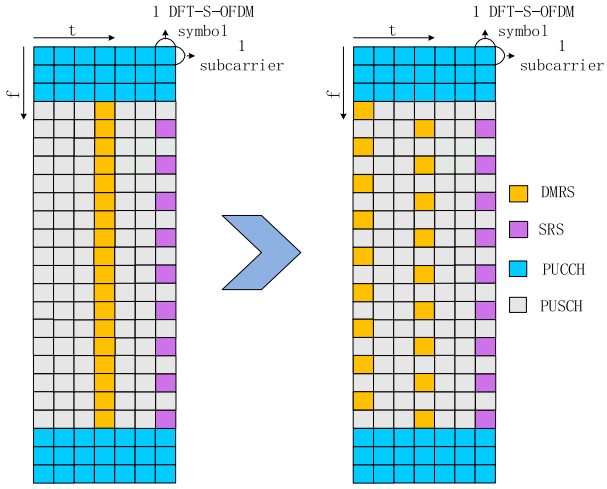

FIGURE 6. The optimization of the DMRS location for processing delay reduction.

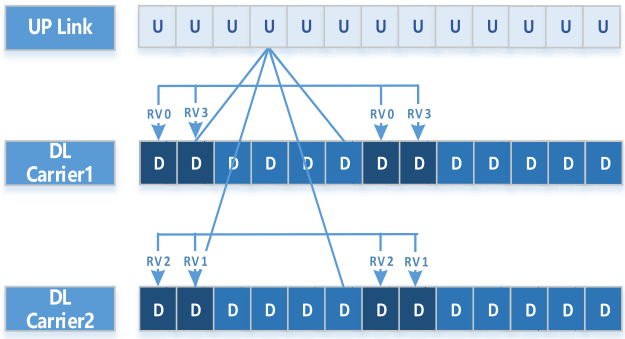

FIGURE 7. The fast retransmission mechanism based on time and frequency bundling.

In the prototype system, the V2V physical channel processing is similar to the physical uplink shared channel (PUSCH) in the NG-RAN platform (see Fig.5). An additional delay optimization for the DMRS is developed. The main reason is that based on the legacy design of the demodulation reference signal (DMRS) for the PUCSH, the BS has to buffer the OFDM symbols of data received before the DMRS symbol and cannot demodulate them until the DMRS being received, which compromises the processing delay. In our prototype system, the DMRS is divided into two parts: the odd part is placed at the first symbol of the slot and the even part remains in the middle. Thus it seems that the BS can obtain the DMRS at the beginning of a subframe and demodulate the data symbol immediately after it being received (see Fig.6). But this effort is not enough, because there is still an obstacle caused by the channel interleaving of PUSCH. In the NG-RAN platform, due to the increasing order that coded bits are written into the interleaving matrix, which is first the column number then the row number, the BS cannot decode the data until it receives all the SC-FDMA symbols of the TTI. This channel interleaving arrangement is disadvantageous for the reduction of the processing delay. A new interleaving method is developed in the prototype system, in which the coded bits are written into the interleaving matrix first the row number, then the column number. Based on the optimizations on the DMRS and interleaving, the BS and VMS can decode the data transmitted on the uplink (V2N) or the sidelink (V2V) immediately after receiving the first DMRS which is very helpful to the reduction of processing delay.

The ultra-reliability mainly depends on the joint design of conservative modulation coding schemes (MSCs) and fast retransmission mechanism. A fast retransmission mechanism based on time and frequency bundling is developed. Firstly, different redundancy versions (RVs) of a TB are transmitted in the first TTI on all available carriers (see Fig.7). If the available carriers in the TTI were not sufficient to transmit

all of the RVs, the residual RVs should be transmitted in the next TTI, repeating this until all the RVs are transmitted. Based on this operation, the developed fast retransmission mechanism can make full use of the multi-carriers resource in the frequency domain to transmit as much as possible RVs. It not only improves the reliability through retransmission technology but also reduces the transmission delay caused by retransmission as much as possible.

2) HIGH TRAFFIC AND HIGH MOBILITY DESIGN

It is a very challenging problem to meet the requirements of high traffic and mobility at the same time. That is because: for high traffic, the cell coverage needs to be as small as possible to reduce the number of terminals competing for bandwidth in a cell; while for high mobility, the cell coverage needs to be as large as possible to avoid the detrimental impact caused by frequent handovers. To cope with this contradiction, a hierarchical heterogeneous network architecture is adopted in the prototype system (see Fig.8). In this architecture, Macro eNodeB (MeNB) is configured with low frequency and high power to extend the coverage of a macro cell, which could avoid system performance degradation with frequent handovers. Meanwhile, there are several small eNodeBs (SeNBs) configured with high frequency and low power within the coverage of MeNBs to provide high system capacity. The V2V communications are allocated dedicated frequency to avoid interference from V2N.

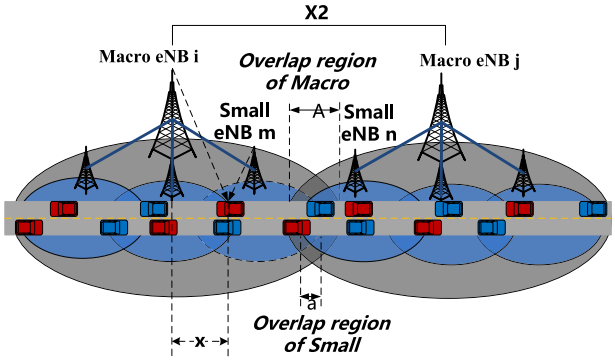

FIGURE 8. The hierarchical heterogeneous network architecture in the prototype system.

Dual connectivity is one of the key technologies to support this architecture, which has been supported in the existing LTE-Advanced pro platform. Base on dual connectivity, serving cells of a user equipment (UE) is composed of two groups, a Master Cell Group (MCG) associated with the MeNB and a Secondary Cell Group (SCG) associated with the SeNB. In the existing SeNB addition/removal method, Radio resource control (RRC) reconfiguration procedure is used to add or remove the serving SeNB of a UE by the serving MeNB. Two RRC messages including RRC reconfiguration and RRC reconfiguration complete need to be exchanged between the UE and MeNB. During this process, data transmission is interrupted. In high mobility scenario, since addition and removal operations happen frequently, the impact of data transmission interruption is more serious.

Combined with the hierarchical heterogeneous network architecture, an improved SeNB addition/removal method based on trajectory prediction is developed in the prototype system. When a UE enters the coverage of a MeNB, several potential serving SeNBs calculated by the result of trajectory prediction are configured to the UE by the MeNB through the RRC configuration procedure. Instead of RRC messages, the MAC control element is used to indicate which SeNB is used for data transmission. With this improved SeNB addition/removal method, the signaling overhead and data interruption caused by high mobility can be mitigated (see Fig.9).

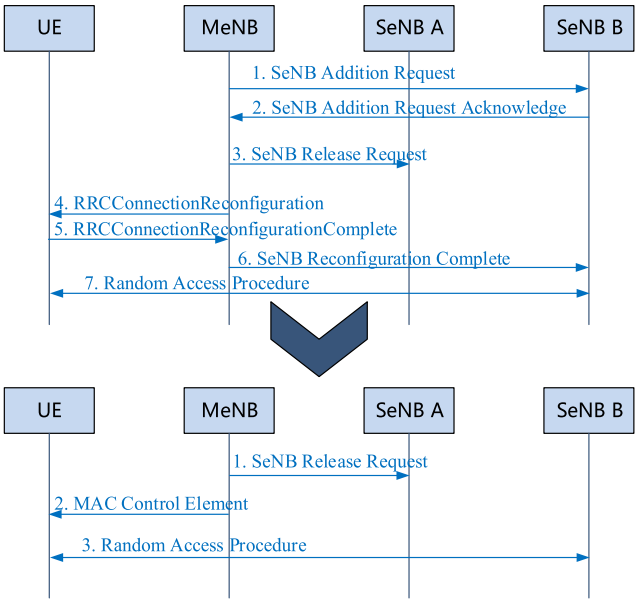

FIGURE 9. The improved SeNB addition/removal method based on trajectory prediction.

The V2X service has a strong localization attribute, which means that the content sent to adjacent vehicles may be the same, such as the local dynamic map (LDM) service and emergency broadcast. Broadcast/multicast technology can distribute the same content to multi-users, which notably have high spectral efficiency. Based on the existing evolved multimedia broadcast multicast service (eMBMS) of the NG-RAN platform, the data gathered from vehicles have to be first transferred to the server outside the core network and then to the eBM-SC of the core network, which is responsible for the broadcast of processed data. The delay caused by traversing the core network makes this mechanism unsuitable for V2X services which are sensitive to the delay. To cope with this problem, in the prototype system, a broadcast/multicast services management entities playing a role similar to the eBM-SC is established within the BS, and an MEC server is deployed close to the BS. A radio bearer of broadcast/multicast services are created between the VMS and BS (see Fig.10). Through this radio bearer,

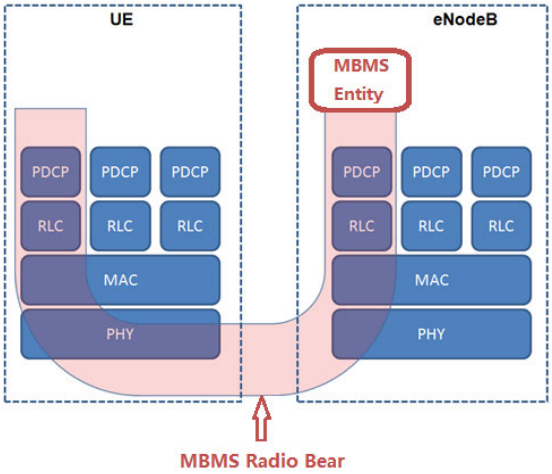

FIGURE 10. Local MBMS entity and MBMS radio bear.

the huge amount of downlink data produced by high precision 3D map dynamic reconstruction service provided by the MEC server can be sent to vehicles in the coverage of a BS more efficiently.

FIGURE 11. The map and real photo of the field tests environment for cooperative autonomous driving oriented 5G-V2X prototype system.

III. FIELD TESTS

A. FIELD TESTS CONFIGURATION

The field tests were conducted at ShanghaiTech University, Shanghai, China. Fig.11 shows the map and real photo of the field tests environment. As shown in Fig.11, there were three sectors located at three sites covering the test route with a length of about 1.3 km. To construct the hierarchical heterogeneous network architecture, cell splitting and cell merging were implemented in these three sectors. Specifically, for a relatively low-frequency carrier, cell merging technology was implemented to make these three sectors form a macro cell to cover the whole test route. Under the coverage of the merged cell, i.e. MeNB in the architecture, handover did not occur on the test route. For the rest higher frequency carriers, cell splitting technology was implemented to form three small cells, i.e. SeNBs in the architecture, to increase network capacity.

FIGURE 12. The network-side devices used in the field tests.

Fig.12 shows the network side devices used in the field tests, including the BBU, MEC server, Core Network, and the RRU and antennas of the three sites. A total of 5 autonomous driving vehicles participated in the field tests. Each vehicle was equipped with an on-vehicle terminal which is developed based on the terminal emulator for 5G-V2X UE (see Fig.13).

FIGURE 13. The autonomous driving vehicles in the platoon and on-vehicle terminals.

A set of high definition (HD) 3D map of the test field was created, which contains all-round elements of the test field such as road lane line and surrounding environment, with an accuracy of 3cm. The location position, azimuth angle, speed, acceleration, and warnings of the vehicle, and

processed perception results base on the on-vehicle sensors were transmitted to the map server for map updating through the V2N link and broadcasted to nearby vehicles through V2V link. The map server dynamically reconstructs the 3D map according to the received information and transmits the reconstructed data to all test vehicles through the optimized MBMS service.

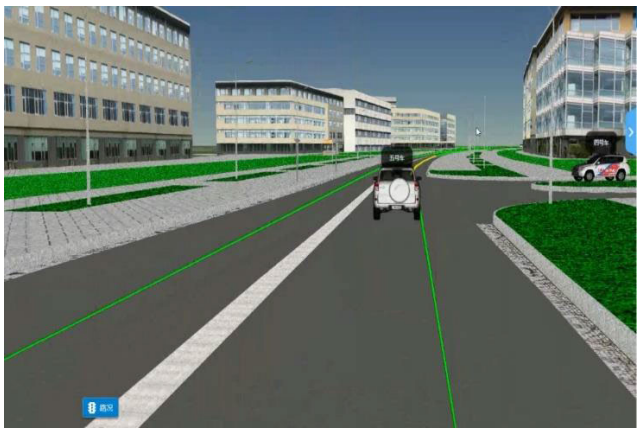

FIGURE 14. The result of a reconstruction of the HD 3D map.

TABLE 2. Major radio parameter of the prototype system for field test.

Radio interface	Between BS and UE		Among UEs
	V2N Downlink	V2N Uplink	V2V Sidelink
Carrier frequency	3.5GHz band		
Bandwith	80MHz	80MHz	20MHz
Multiple access	OFDMA		
TTI length	0.125ms (7 OFDM symbols)		
Duplex	Time Division Duplexing (TDD)		
Scheduling	Round Robin		Semi-persistent
Tx antenna ports	8Tx	2Tx	2Tx
Rx antenna ports	2Rx	8Rx	2Rx
Retransmission	HARQ + Time and frequency bundling		

Fig.14 shows the result of a dynamic reconstruction of the HD 3D map.

TABLE 2 summarizes the major radio parameters of the prototype system.

B. FIELD TEST PROCESS AND RESULTS

Field tests were conducted to achieve the following two goals: (1) to evaluate whether the key performance indicators (KPIs) of the prototype system meet the strict QoS requirements; (2) to verify the promotion effect of 5G-V2X on autonomous driving. For the first goal, performance tests were conducted to evaluate the end-to-end delay, reliability, and throughput of V2X links. For the second goal, functional tests of cooperative autonomous driving technologies such as cooperative lane changing, real-time map updating and path planning were performed.

In the first test case, an autonomous driving vehicle traveled along the test route at a speed of 30-60km/h. Using Xcap

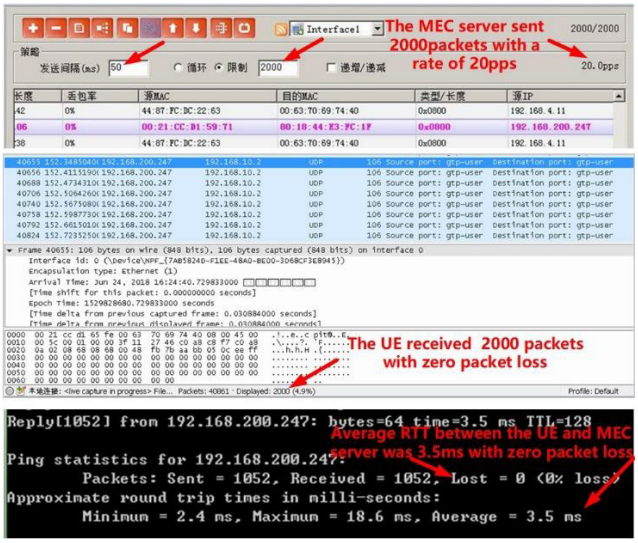

FIGURE 15. Test results for the reliability and delay of the V2N link.

software, the MEC server sent data packets with a rate of 20packets per second (PPS) to the vehicle, with a size of 64 bytes. The vehicle then continuously sent ping packets to the MEC server with a size of 64 bytes. Fig.15 shows the test result. It can be seen that the MEC server sent a total of 2000 data packets to the UE on the test vehicle with zero packet loss. The average Round Trip Time (RTT) between the UE and the MEC server was 3.5ms, and the minimum is 2.4ms. None of the ping packets were lost. It should be noted that RTT is twice the end-to-end delay, and V2V physical channel processing is the same as PUSCH, so the results prove that V2N and V2V of the prototype system can meet the 5G-V2X QoS requirements in terms of low latency (3ms) and high reliability (99.999%).

The second test case was mainly for rate evaluation. In the first step, five autonomous driving vehicles traveled along the test route at a speed of 30-60km/h, and simultaneously download data from the MEC server using ftp software. One rate sampling point was recorded every 250ms using IPOP software. Fig.16 shows the cumulative distribution function (CDF) of download rate samples for each vehicle. It can be seen that each vehicle achieved a download rate of more than 50 Mbps over 95% of the time. In the second step, the two autonomous driving vehicles were 200m apart. The front vehicle used XCAP software to generate full buffer data and broadcast them to the rear vehicle, to test the receiving rate of the rear vehicle. To ensure the reliability, each transmission block was transmitted 4 times fixedly, corresponding to redundant versions 0, 2, 3, and 1 in turn. The test results are shown in Fig.17. It can be seen that the generation rate of the data source of the front car is 34.7mbps, and the reception rate of the rear car is 14.7mbps. These results show that to a certain extent, this field test system can provide services that meet the 5G-V2X QoS requirements in terms of data rate.

The third test case was mainly to evaluate the cooperative autonomous driving function enabled by 5G-V2X.

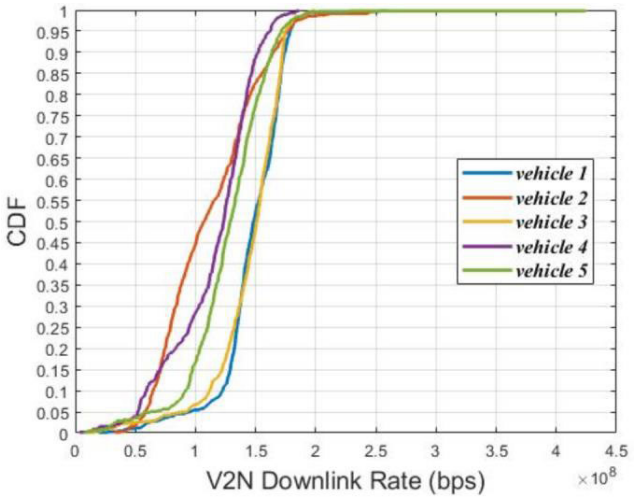

FIGURE 16. The CDF of downlink rate samples with each vehicle.

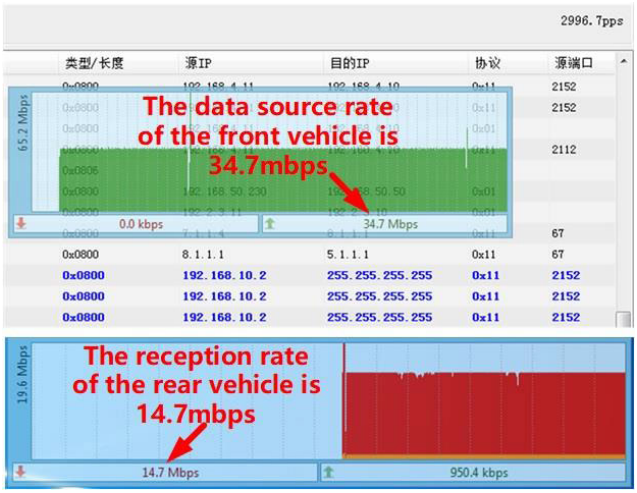

FIGURE 17. V2V reception rate between two vehicles 200m apart.

A cooperative scenario of five autonomous driving vehicles supported by 5G-V2X and HD 3D dynamic map was designed (see Fig.18).

In the design of this scenario, vehicle 1 simulated a fault during driving, gradually decelerated and stopped, broadcast the current speed and position through V2V, and reported to the map server through V2N. Located within the V2V communication range of vehicle 1, vehicle 4 received the broadcast, slowed down and changed lanes with the cooperation of vehicle 2. Vehicle 3 found the temporary construction blocking of the road ahead, broadcast the information through V2V, and reported it to the map server through V2N. After receiving the V2V broadcast, vehicle 2 began to slow down gradually. The map server sent an incremental update message to all vehicles after real-time map reconstruction of the new information received. Although vehicle 5 was not within the V2V communication range of vehicle 1 and vehicle 3, it could still sense these abnormal events in a very

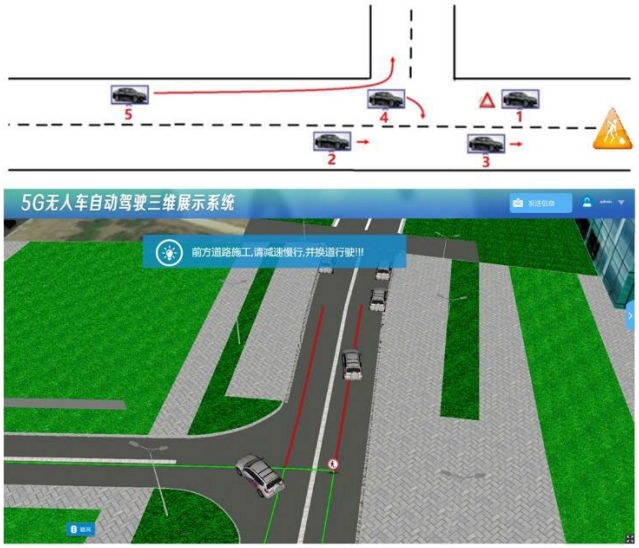

FIGURE 18. The cooperative scenario of five autonomous driving vehicles supported by the 5G-V2X prototype system and HD 3D dynamic map.

short time through the dynamically updated HD 3D map, and then re-planed the path to turn at the intersection to avoid the blocked road. The actual test results are basically consistent with the scenario design. The effect can be seen in the 3D map display system shown in Fig.18. The test result proves that with the support of 5G-V2X and HD 3D dynamic map, the cooperative autonomous driving technology can effectively solve the shortcomings of limited perception range and lack of collaborative maneuvers in the traditional autonomous driving technology.

The field test results prove that the prototype system achieved the design goals, and 5G-V2X has a significant promotion effect on autonomous driving technology. However, it can also be seen that in order to meet the requirements of ultra-reliable, low latency, high traffic, and high mobility, a large investment in resources such as equipment and frequency is required. As mentioned in the introduction part, there is an urgent need for some optimization tools to reduce CAPEX and OPEX costs during the commercial deployment of 5G-V2X. Besides, some optimization tools are needed to promote the research work of 5G-V2X evolution, such as the introduction of multi-hop technology and cognitive radio technology with the effect of expanding the V2V communication range and increasing frequency resources.

IV. AI-BASED OPTIMIZATION TOOLS

A. DEEP LEARNING BASED PST-RESNET

1) PROBLEM DEFINITION

As described in the introduction, accurate user and network traffic prediction are of great significance to reduce CAPEX and OPEX of the 5G-V2X system. Simultaneously forecasting the number of users or the network traffic of each cell of a city-wide 5G-V2X network, however, is very challenging, affected by the three complex factors including spatial

dependencies, temporal dependencies and external influence such as weather conditions and events. Junbo Zhang *et al* constructed deep spatio-temporal residual networks (ST-ResNet) for city-wide crowd flows prediction in [22]. ST-ResNet can segment the regions of a city into a regular grid structure, and then give the prediction results of each grid. In the prediction of spatio-temporal data in city-wide regions, ST-ResNet shows good performance. However, in general, because all the cells of the 5G-V2X network cannot form a regular grid structure, ST-ResNet cannot be used directly to solve our prediction problem. To this end, based on ST-ResNet, we construct a tool called deep spatio-temporal residual networks with a permutation operator (PST-ResNet), which can predict spatio-temporal data for not only grid based segmentation but also irregular segmentation (see Fig.19).

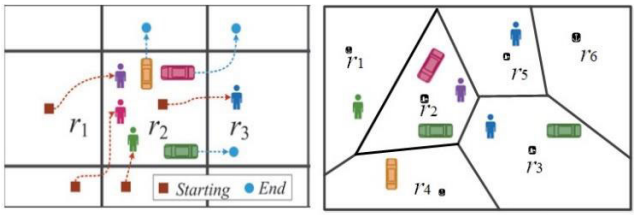

FIGURE 19. PST-ResNet supports not only grid based segmentation but also irregular segmentation.

We assume that the city-wide 5G-V2X network is segmented into N regions and the region group is a finite set $\boldsymbol{\Omega} = \{\boldsymbol{r_1}, \boldsymbol{r_2}, \cdots, \boldsymbol{r_N}\}$. Each region $\boldsymbol{r_i}$ has a geospatial position and time-varying attributes $\boldsymbol{C}$. The time-varying attributes $\boldsymbol{C}$ can be defined differently depending on the task and types of spatio-temporal data, e.g. the user number, the network traffic, or the inflow and outflow defined in [22]. At the $\boldsymbol{t^{\text{th}}}$ time interval, the time-varying attributes $\boldsymbol{C}$ of all regions can be denoted as a tensor $\boldsymbol{V_t^0} \in \boldsymbol{R^{\Omega \times C}}$, where $\boldsymbol{V_t^0} = [\boldsymbol{V_{t,r_1}^0}, \boldsymbol{V_{t,r_2}^0}, \cdots \boldsymbol{V_{t,r_N}^0}]$. Thus, the observation of attributes at any time can be represented by an attribute tensor $\boldsymbol{V^0} = [\boldsymbol{V_{r_1}^0}, \boldsymbol{V_{r_2}^0}, \cdots, \boldsymbol{V_{r_N}^0}]$.

Problem 1: Given $\left\{\boldsymbol{V_t^0} \,|\, \boldsymbol{t} = 0, \cdots, \boldsymbol{n-1}\right\}$ as the historical observations, predict $\boldsymbol{V_n^0}$.

2) METHODOLOGY

In the grid based segmentation method adopted by [22], since the finite set $\boldsymbol{\Omega}$ can be represented by an $\boldsymbol{I} \times \boldsymbol{J}$ matrix, where $\boldsymbol{I}$ and $\boldsymbol{J}$ are the number of rows and columns of the grid respectively, convolution-based residual networks can be used to model nearby and distant spatial dependencies between any two regions in a city. In the case of more general irregular segmentation, the finite set $\boldsymbol{\Omega}$ cannot be represented directly by a matrix, which leads to the failure of convolution-based residual networks. To solve this problem, we introduce a permutation operator to reconstruct the set $\boldsymbol{\Omega}$ into a matrix form, so as to reuse the proven effective network architecture of ST-ResNet.

The permutation function σ for $\boldsymbol{\Omega}$ can be expressed by (1), where $\boldsymbol{i_1}, \boldsymbol{i_2}, \cdots, \boldsymbol{i_N}$ is an arrangement of $\boldsymbol{1}, \boldsymbol{2}, \cdots, \boldsymbol{N}$.

$$\boldsymbol{\sigma} = \begin{pmatrix} \boldsymbol{r_1}, \boldsymbol{r_2}, \cdots, \boldsymbol{r_N} \\ \boldsymbol{r_{i_1}}, \boldsymbol{r_{i_2}}, \cdots, \boldsymbol{r_{i_N}} \end{pmatrix} \tag{1}$$

We define the permutation operator $\boldsymbol{P_M}$ as a set of permutation functions, i.e. $\boldsymbol{P_M} = \{\boldsymbol{\sigma_1}, \boldsymbol{\sigma_2}, \cdots, \boldsymbol{\sigma_M}\}$. After $\boldsymbol{M}$ times permutation operations using $\boldsymbol{P_M}$, $\boldsymbol{\Omega}$ becomes an $(\boldsymbol{M}+\boldsymbol{1}) \times \boldsymbol{N}$ matrix. Fig.20 shows an example in which an irregular segmentation region group is transformed into a matrix form after permutation. Fig.20 shows the difference in the process and result of generating the final $\boldsymbol{\Omega}$ for the grid based segmentation supported by ST-RESNET and the irregular segmentation supported by PST-RESNET for the same area.

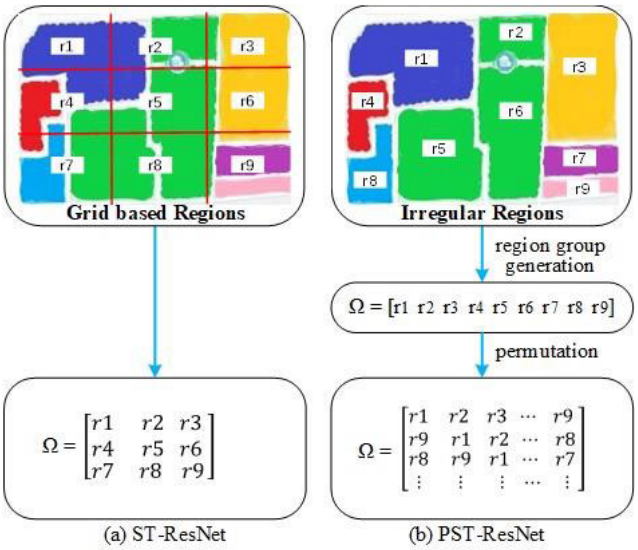

FIGURE 20. The difference in the process and result of generating the final Ω between ST-ResNet and PST-ResNet.

For the $(\boldsymbol{K}+\boldsymbol{1}) \times \boldsymbol{N}$ order $\boldsymbol{\Omega}$ matrix obtained by $\boldsymbol{K}$ times of permutation operation of the original region group, its corresponding attribute tensor $\boldsymbol{PX^K}$ can be expressed by (2), where $\boldsymbol{V^k} = \left[\boldsymbol{V_{r_{i_1}}^k}, \boldsymbol{V_{r_{i_2}}^k}, \cdots, \boldsymbol{V_{r_{i_N}}^k}\right]$ and $\boldsymbol{V_{r_{im}}^k}$ is the attribute corresponding to region $\boldsymbol{r_{i_m}}$.

$$\boldsymbol{PX^K} = \left[\boldsymbol{V^0}, \boldsymbol{V^1}, \cdots, \boldsymbol{V^K}\right]^{\mathrm{T}}, \quad \boldsymbol{PX^K} \in \boldsymbol{R^{(K+1)\times N \times C}} \tag{2}$$

Then the **problem 1** is transformed into: Given $\left\{\boldsymbol{PX_t^K} \,|\, \boldsymbol{t} = \boldsymbol{0}, \cdots, \boldsymbol{n-1}\right\}$ as the historical observations, predict $\boldsymbol{PX_n^K}$. Fig.21 shows an observed instance of the attribute of regions in a city area and the instance after region group generation and permutation. The instance after permutation is a $\boldsymbol{PX_t^K}$.

In PST-ResNet, we use the same network structure as ST-ResNet, which can be seen in Fig.22. The difference is that the input of PST-ResNet is the attribute matrix sequence being permutated, while the input of PST-ResNet is the original attribute matrix sequence. In the temporal hand, the time axis is divided into three fragments, denoting recent

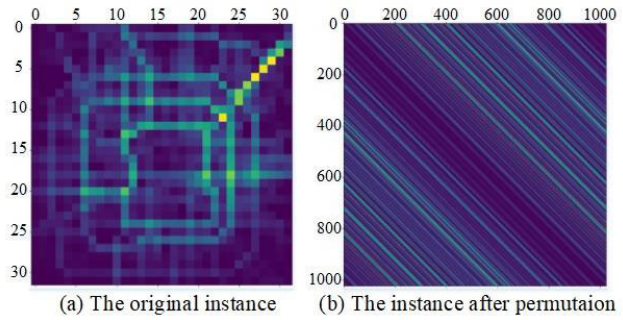

FIGURE 21. An observed instance of the attribute of regions in a city area and the instance after region group generation and permutation.

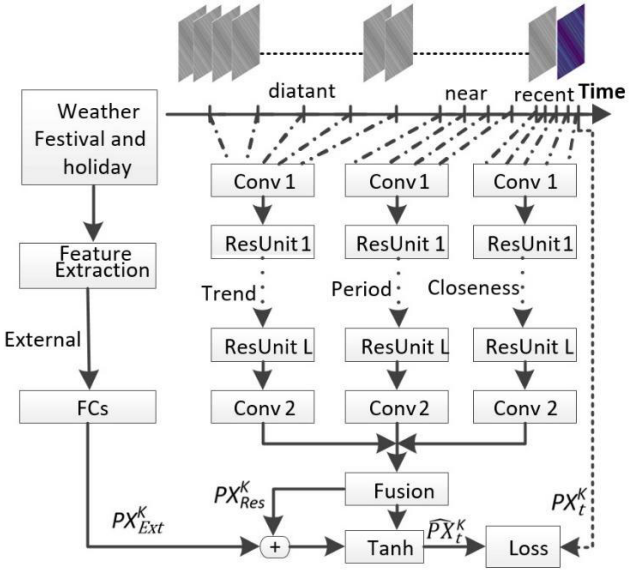

FIGURE 22. PST-ResNet architecture. Conv: Convolution; ResUnit: Residual Unit; FC: Fully-connected.

time, near history and distant history. The attribute tensors of intervals in each time fragment are then fed into three components separately to model the three temporal properties: closeness, period and trend, respectively. The three components (i.e. closeness, period, and trend) share the same network structure, which is composed of two subcomponents: convolution and residual unit. In the external component, some features from external datasets, such as weather conditions and events are manually extracted and fed into a two-layer fully-connected neural network. Finally, the aggregation is mapped into $[-1; 1]$ by a Tanh function. More details on the components of this architecture can be found in [22].

The three attribute tensors of the time fragments are $\left[\boldsymbol{PX}^{K}_{t-l_c}, \boldsymbol{PX}^{K}_{t-(l_c-1)}, \cdots, \boldsymbol{PX}^{K}_{t-1}\right]$, $[\boldsymbol{PX}^{K}_{t-l_p\cdot p}, \boldsymbol{PX}^{K}_{t-(l_p-1)\cdot p}, \cdots, \boldsymbol{PX}^{K}_{t-p}]$, and $[\boldsymbol{PX}^{K}_{t-l_p\cdot q}, \boldsymbol{PX}^{K}_{t-(l_q-1)\cdot q}, \cdots, \boldsymbol{PX}^{K}_{t-q}]$, where $\boldsymbol{l_c}$, $\boldsymbol{l_p}$ and $\boldsymbol{l_q}$ are the length of the *closeness* dependent sequence, the *period* dependent sequence and the *trend* dependent sequence respectively. The attribute tensor is followed by a convolution (i.e. Conv1 shown in Fig.22) as:

$$\boldsymbol{PX}^{\boldsymbol{K}^{(1)}} = \boldsymbol{f}\left(\boldsymbol{W}^{(1)} * \boldsymbol{PX}^{\boldsymbol{K}^{(0)}} + \boldsymbol{b}^{(1)}\right) \tag{3}$$

where $*$ denotes the convolution; $\boldsymbol{f}$ is an activation function e.g. the rectifier $\boldsymbol{f}(z) = \boldsymbol{max}(\boldsymbol{0}, z)$, $\boldsymbol{W}^{(1)}$ and $\boldsymbol{b}^{(1)}$ are the learnable parameters in the first layer.

We stack $\boldsymbol{L}$ residual units following Conv1 as:

$$\boldsymbol{PX}^{\boldsymbol{K}^{(l+1)}} = \boldsymbol{PX}^{\boldsymbol{K}^{(l)}} + \mathcal{F}\left(\boldsymbol{PX}^{\boldsymbol{K}^{(l)}}; \boldsymbol{\theta}^{(l)}\right), \quad \boldsymbol{l} = \boldsymbol{1}, \cdots \boldsymbol{L} \tag{4}$$

where $\mathcal{F}$ is the residual function (i.e. two combinations of "ReLU + Convolution"), and $\boldsymbol{\theta}^{(l)}$ includes all learnable parameters in the $\boldsymbol{l}^{\mathbf{th}}$ residual unit. The Lth residual unit is followed by a convolutional layer (i.e. Conv2 shown in Fig.22). The outputs of the Conv2s of the three components are $\boldsymbol{PX}_c^{\boldsymbol{K}^{(L+2)}}$, $\boldsymbol{PX}_p^{\boldsymbol{K}^{(L+2)}}$, and $\boldsymbol{PX}_q^{\boldsymbol{K}^{(L+2)}}$ respectively. The three outputs are fused as follows

$$\boldsymbol{PX}^{\boldsymbol{K}}_{\boldsymbol{Res}} = \boldsymbol{W}_c \circ \boldsymbol{PX}_c^{\boldsymbol{K}^{(L+2)}} + \boldsymbol{W}_p \circ \boldsymbol{PX}_p^{\boldsymbol{K}^{(L+2)}} + \boldsymbol{W}_q \circ \boldsymbol{PX}_q^{\boldsymbol{K}^{(L+2)}} \tag{5}$$

where $\circ$ is Hadamard product (i.e. element-wise multiplication), and $\boldsymbol{W}_c$, $\boldsymbol{W}_p$, and $\boldsymbol{W}_q$ are the learnable parameters that adjust the degrees affected by closeness, period and trend, respectively.

Finally, the predicted value at the $\boldsymbol{t^{th}}$ time interval, denoted by $\widehat{\boldsymbol{PX}}_{\boldsymbol{t}}^{\boldsymbol{K}}$ is defined as

$$\widehat{\boldsymbol{PX}}_{\boldsymbol{t}}^{\boldsymbol{K}} = \boldsymbol{tanh}(\boldsymbol{PX}^{\boldsymbol{K}}_{\boldsymbol{Res}} + \boldsymbol{PX}^{\boldsymbol{K}}_{\boldsymbol{Ext}}) \tag{6}$$

where $\boldsymbol{tanh}$ is a hyperbolic tangent that ensures the output values are between -1 and 1. It should be noted that $\widehat{\boldsymbol{PX}}_{\boldsymbol{t}}^{\boldsymbol{K}}$ is actually $\left[\widehat{\boldsymbol{V}}^{\boldsymbol{0}}, \widehat{\boldsymbol{V}}^{1}, \cdots, \widehat{\boldsymbol{V}}^{K}\right]^{\mathrm{T}}$. We can get the final solution of the original **problem 1** by averaging the elements corresponding to the same region $\boldsymbol{r_i}$ in $\left[\widehat{\boldsymbol{V}}^{\boldsymbol{0}}, \widehat{\boldsymbol{V}}^{1}, \cdots, \widehat{\boldsymbol{V}}^{K}\right]^{\mathrm{T}}$. Our PST-ResNet can be trained to predict $\boldsymbol{PX}_{\boldsymbol{t}}^{\boldsymbol{K}}$ by minimizing the mean squared error between the $\widehat{\boldsymbol{PX}}_{\boldsymbol{t}}^{\boldsymbol{K}}$ and $\boldsymbol{PX}_{\boldsymbol{t}}^{\boldsymbol{K}}$:

$$\mathcal{L}(\boldsymbol{\theta}) = \left\| \boldsymbol{PX}_{\boldsymbol{t}}^{\boldsymbol{K}} - \widehat{\boldsymbol{PX}}_{\boldsymbol{t}}^{\boldsymbol{K}} \right\| \tag{7}$$

where $\boldsymbol{\theta}$ are all learnable parameters in the PST-ResNet. Algorithm 1 outlines the PST-ResNet training process. We first transform every training instance by a permutation operator (line 1) and then construct the training instances from the permutated sequence data (lines2-7). After that, PST-ResNet is trained (lines 8-12) via backpropagation and Adam [38].

B. SWARM INTELLIGENCE BASED SC-DSCS

As one of the popular swarm intelligence tools, cuckoo search (CS) is powerful for solving complex global optimization problems and has been successfully applied to the researches of V2X related technology. However, CS is a highly random search by employing the Levy flight mechanism, and information of good nest locations (solutions) that have been found is not fully utilized in the search process. The step length does not change according to the position of the nest due to the

Algorithm 1 PST-ResNet Training Algorithm

Input: Historical observations: $\left\{V_0^0, V_1^0, \cdots, V_{n-1}^0\right\}$
external features: $\{E_0, \cdots, E_{n-1}\}$
lengths of closeness, period, trend sequences: l_c, l_p, and l_q
period: p; trend q.
Output: Learned PST-ResNet model

// permutation operation
Permutate $\left\{V_0^0, V_1^0, \cdots, V_{n-1}^0\right\}$ **into** $\left\{PX_t^K \mid \mathbf{t} = \mathbf{0}, \cdots, \mathbf{n-1}\right\}$
$\mathcal{D} \longleftarrow \emptyset$
for *all available time interval* $t(1 \le t \le n-1)$ **do**
  $\mathcal{S}_c = \left[PX_{t-l_c}^K, PX_{t-(l_c-1)}^K, \cdots, PX_{t-1}^K\right]$
  $\mathcal{S}_p = [PX_{t-l_p \cdot p}^K, PX_{t-(l_p-1)\cdot p}^K, \cdots, PX_{t-p}^K]$
  $\mathcal{S}_q = [PX_{t-l_p \cdot q}^K, PX_{t-(l_q-1)\cdot q}^K, \cdots, PX_{t-q}^K]$
  //PX_t^K is the target at time t
  put an training instance($\{\mathcal{S}_C, \mathcal{S}_p, \mathcal{S}_q, E_t\}, PX_t^K$) into $\mathcal{D}$
// train the model
initialize all learnable parameters θ in PST-ResNet
  repeat
    randomly select a batch of instances $\mathcal{D}_b$ from $\mathcal{D}$
    find θ by minimizing the objective (7) with $\mathcal{D}_b$
  until stopping criteria is met

fixed step length control mechanism, which results in a lack of adaptability. These defects limit the performance of CS in convergence efficiency. In order to improve the convergence rate and optimization precision of CS, we proposed the subpopulation collaboration based dynamic self-adaption cuckoo Search (SC-DSCS) in [39]. In this paper, the specific steps of SC-DSCS are briefly described, and some evaluation results of computational complexity are added.

The specific steps of SC-DSCS are described as follows.

Step 1: Initialization setting. There is a population of N birds, and N nest locations (solutions) $X_t = \left\{x_1^t, x_2^t, \cdots, x_N^t\right\}, t = 0$. Then a special subpopulation consists of M birds is isolated from the population.

Step 2: Optimal nest sequence generation. The N nest locations X_t are arranged in descending order in terms of the fitness value (objective function value). The first K elements are extracted to form the optimal nest sequence $X_{Best}^t = \{x_{best_1}^t, x_{best_2}^t, \cdots, x_{best_K}^t, x_{new}^t$,where x_{new}^t is calculated according to (8), and $K < M$. The remaining nest sequence is $X_{Res}^t = \{x_{res_1}^t, x_{res_2}^t, \cdots, x_{res_{N-K}}^t\}$.

$$x_{new}^t = 1/3\left(\lambda_1 * x_{best_1}^t + \lambda_2 * x_{best_2}^t + \lambda_{13} * x_{best_3}^t\right) \quad (8)$$

Step 3: Searching operation. The N birds update their nest locations according to (9-13). For each of the M birds in the special subpopulation, the start location x_i^t is successively chosen from X_{Best}^t in a round-robin manner. For the rest (N-M) birds in the population, each bird chooses a different element in the X_{Res}^t as the start location x_i^t. α_{min} and α_{max} are the minimum step length control and maximum step length control respectively. d_{max} is the maximum distance between x_{new}^t and other nest locations. During Levy flight, the search direction is uniformly distributed, and the search step length s is obtained by Mantegna's algorithm, which is given in (12), where u and v obey the normal distribution, i.e. $u \sim N\left(0, \sigma_u^2\right)$, $v \sim N\left(0, \sigma_v^2\right)$, and $\sigma_u = 1$. σ_v is calculated by (13), where $\Gamma(1+\beta)$ is the gamma function, and $1 < \beta \le 3$. Then, compare the fitness of X_t, x_{new}^t and X_{t+1}. The best nest location x_{best}^{t+1} is chosen and entered the next step.

$$x_i^{t+1} = x_i^t + \alpha_j \otimes Levy(\lambda) \quad (9)$$

$$\alpha_j = \alpha_{min} + (\alpha_{max} - \alpha_{min}) d_i \quad (10)$$

$$d_i = \frac{\left\|x_i^t - x_{new}^t\right\|}{d_{max}} \quad (11)$$

$$s = \frac{u}{|v|^{1/\beta}} \quad (12)$$

$$\sigma_v = \left\{\frac{\Gamma(1+\beta)\, sin(\pi\beta/2)}{\Gamma\left[(1+\beta)/2\right]\beta 2^{(\beta-1)/2}}\right\}^{1/\beta} \quad (13)$$

Step 4: Selection of nest locations. Generate the random number $r \in [0, 1]$, which obeys the uniform distribution. Contrast it with the detection probability $Pa = 0.25$. If $r > Pa$, change x_i^{t+1} randomly, otherwise unchanged. Test the changed nest locations, compare them with locations of the last step and update the best nest location x_{best}^{t+1}.

Step 5: Judgment operation. Calculate the fitness value of x_{best}^{t+1} and judge whether it achieves the termination condition. If it is satisfied, x_{best}^{t+1} is the optimal solution, otherwise, return to step 2 and start the next iteration.

It can be found from the above steps that unlike all birds in the original CS, which perform the same search rules, a special subpopulation is isolated in SC-DSCS, which will make the best use of good nest locations, and an additional new nest location is created based on the comprehensive assessment of the first three best nests, the idea of which is borrowed from Grey Wolf Optimizer (GWO) that the alpha (best candidate solution), beta and delta have better knowledge about the potential location of prey (see step2). Adaptive step length control is adopted to improve the adaptability of SC-DSCS (see step 3).

V. EVALUATIONS OF PST-RESNET AND SC-DSCS

A. PST-RESNET

It can be seen from Fig. 21 that PST-ResNet is not sensitive to how the regions are segmented. Therefore, we can use the data set provided in [22] for evaluating ST-ResNet to evaluate PST-ResNet. The advantage of this is that the existing results of ST-RESNET can provide a reference for the performance evaluation of PST-ResNet.

The TaxiBJ dataset (see Table 3) is used to predict the inflow and outflow of each region in the 32 × 32 grid

TABLE 3. Dataset (holidays include adjacent weekends).

Dataset	TaxiBJ
Data type	Taxi GPS
Location	Beijing
Time Span	7/1/2013 - 10/30/2013 3/1/2014 - 6/30/2014 3/1/2015 - 6/30/2015 11/1/2015 - 4/10/2016
Time interval	30 minutes
Gird map size	(32, 32)
Trajectory data	
Average sampling rate (s)	~ 60
# taxis	34,000+
# available time interval	22,459
External factors (holidays and meteorology)	
# holidays	41
Weather conditions	16 types (e.g., Sunny, Rainy)
Temperature / ◦C	[−24.6, 41.0]
Wind speed / mph	[0, 48.6]

regions of Beijing. It means that in this evaluation, the time-varying attributes $\boldsymbol{C}$ are inflow and outflow, which are the number of taxi entering and leaving a region over 30 minutes. TaxiBJ dataset includes trajectory data of the taxicab GPS and meteorology data in Beijing from four time intervals: 1st Jul. 2013 - 30th Otc. 2013, 1st Mar. 2014 - 30th Jun. 2014, 1st Mar. 2015 - 30th Jun. 2015, 1st Nov. 2015 - 10th Apr. 2016. The data processing and the selection of hyperparameters are the same as those of ST-ResNet (For details, see [22]). The difference is that based on the processed data in the ST-ResNet evaluation, we first convert the 32×32 inflow and outflow matrices corresponding to each time interval into two 1×1024 vectors, and then carry out 9 times (i.e. $\boldsymbol{K} = 9$) of permutation operations and transform the inflow and outflow matrices into 10×1024. In order to compare the impact of different permutations on the prediction results, we select $1 \times 1024, 2 \times 1024, \cdots, 10 \times 1024$ elements from the 10×1024 matrices to form training samples, so as to obtain different models and prediction performance.

We first give the result of PST-ResNet on TaxiBJ under different models and the number of permutations, as shown in Table 4.

The evaluation Metric is also the root mean square error (RMSE). We give 4 variants of PST-ResNet with different layers and different factors. Taking L12-E for example, it considers all available external factors and has 12 residual units, each of which is comprised of two convolutional layers. Based on the results in Table 4, it is not that the larger $\boldsymbol{K}$ is, the better the prediction accuracy is. We need to try different permutations to get better prediction results and models.

We compare the results of our PST-ResNet with the results of other 6 baselines (including HA, ARIMA, SARIMA, VAR, SA-ANN, and DeepST) and ST-ResNet provided by [22], as shown in Table 5. The best error result of ST-ResNet given in [22] is 16.69, while PST-ResNet further reduces it to 13.37. The reason why ST-ResNet can achieve better prediction accuracy than baselines is partly that the network architecture design considers the spatial dependency between

TABLE 4. Result of PST-ResNet on TaxiBJ under different models and number of permutations.

Model	# Permutation	RMSE
L2-E 2 residual units +E	1*1024	20.427426
	2*1024	18.42872
	3*1024	18.346954
	4*1024	15.908107
	5*1024	18.387142
	6*1024	**14.698557**
	7*1024	14.868666
	8*1024	14.991085
	9*1024	15.643366
	10*1024	19.02592
L4-E 4 residual units +E	1*1024	20.341682
	2*1024	21.042808
	3*1024	20.741211
	4*1024	14.764576
	5*1024	21.187219
	6*1024	14.364003
	7*1024	14.496468
	8*1024	14.479627
	9*1024	**14.305274**
	10*1024	20.949730
L12-E 12 residual units +E	1*1024	18.079021
	2*1024	17.904785
	3*1024	17.963238
	4*1024	**13.732718**
	5*1024	18.181012
	6*1024	15.135051
	10*1024	17.984308
L12-E-BN L12-E with BN	1*1024	31.630377
	2*1024	21.171398
	3*1024	22.103576
	4*1024	**16.076698**
	5*1024	22.122469
	6*1024	23.271779
	7*1024	17.100171
	8*1024	17.512258

TABLE 5. Comparison among different methods on TaxiBJ.

Model		RMSE	
HA		57.69	
ARIMA		22.78	
SARIMA		26.88	
VAR		22.88	
ST-ANN		19.57	
DeepST		18.18	
		RMSE of ST-ResNet	**RMSE of PST-ResNet**
L2-E	2 residual units +E	17.67	14.70
L4-E	4 residual units +E	17.51	14.31
L12-E	12 residual units +E	16.89	**13.73**
L12-E-BN	L12-E with BN	**16.69**	16.08

different regions, so it could be inferred that although the replacement operation disrupts the arrangement relationship of different regions, the space dependencies can still be captured by PST-ResNet. Permutation statistical methods are data-dependent and provide either exact or highly-accurate approximate probability values [40]. This may be why PST ResNet performs better.

The evaluation results show that by introducing the permutation operator, PST-ResNet not only solves the problem that ST-ResNet cannot be applied to the prediction of spatio-temporal data in the case of irregular segmentations but

TABLE 6. Evaluation of computational complexity.

Function	Value	Running Time (second)			SC-DSCS/ RC-SSCS (%)
		RC-SSCS	SC-DSCS-noGW	SC-DSCS	
F1	1.0e-4	3.236409	1.328003	1.113347	34.4
F2	1.0e-4	–	13.999284	11.5888788	–
F3	1.0e-4	10.055612	2.076678	1.866048	18.56
F4	1.0e-4	40.557214	26.025856	20.710596	51.07
F5	1.0e-4	8.598201	1.255973	1.225573	14.25
F6	-20	10.4654114	6.855324	6.254782	59.77
F7	1.0e-3	82.042343	28.855642	23.787590	28.99
F8	-10000	–	3.532125	3.407619	–
F9	1.0e-4	6.403412	3.984976	3.458	54.00

also further improves the prediction accuracy of ST-ResNet, which makes PST-ResNet a powerful tool for 5G-V2X network optimization.

B. SC-DSCS

The performance of SC-DSCS has been evaluated based on nine benchmark functions in [39]. Compared with CS, PSO, ABC, and DE, experimental results show that the SC-DSCS algorithm has better convergence speed and optimization precision. The comparison results of SC-DSCS and RC-SSCS proposed in [37] in terms of computational complexity are given here. In order to make the evaluation result of computational calculation complexity more intuitionistic, the running time required for the algorithm to search the specified precision value is compared under the same running environment (a PC running Matlab). The shorter the running time is, the higher the efficiency of the algorithm is. The nine benchmark functions are the same as in [39].

Results are shown in Table 6. SC-DSCS-noGW means SC-DSCS without Grey Wolf (i.e. without $\boldsymbol{x}_{new}^{t}$). In F2 function evaluation, RC-SCCS cannot reach the accuracy value of 1.0e-4 within a preset time limit and converges to 21.53 when the average operation is 54.2s. In F8 function evaluation, RC-SCCS cannot converge to -10000 within a preset time limit and can converge to -7000 at an average running time of 4.2s, and to 17.50 at 17.88s. It can be seen from the running time ratio of SC-DSCS and RC-SSCS that SC-DSCS is significantly better than RC-SSCS. SC-DSCS performs slightly better than SC-DSCS-noGW. Existing evaluation results show that SC-DSCS is an excellent CS variant, which provides a powerful tool for solving complex optimization problems in subsequent research of 5G-V2X.

VI. CONCLUSION

In this paper, we present a cooperative autonomous driving oriented MEC-aided 5G-V2X prototype system design, the rationale behind the design choices and the field test results of the prototype system. As we have demonstrated, the combination of 5G-V2X, MEC and cooperative autonomous driving can be pretty powerful. In order to reduce the CAPEX and OPEX costs of the commercial 5G-V2X networks and solve the complex optimization problems in the subsequent researches, we proposed the PST-ResNet and SC-DSCS, which are two widely adaptive AI-based tools. The evaluation results verify the excellent performance of these two tools. In the future, we will try to introduce cognitive radio, multi-hop communication, and other technologies into our experimental system, and use permutation static methods and Markov chain framework to analyze these two tools theoretically.

REFERENCES

[1] *Service requirements for V2X services (v15.0.0, Release 15)*, document 3GPP TS 22.185, 3GPP, Jun. 2018.

[2] H. Hartenstein and K. Laberteaux, *VANET: Vehicular Applications and Inter-Networking Technologies*. Hoboken, NJ, USA: Wiley, 2009.

[3] B. Sharma, M. S. P. Sharma, and R. S. Tomar, "A survey: Issues and challenges of vehicular ad hoc networks (VANETs)," in *Proc. Int. Conf. Sustain. Comput. Sci., Technol. Manage. (SUSCOM)*, Amity Univ. Rajasthan, Jaipur: India, Feb. 2019. [Online]. Available: https://ssrn.com/abstract=3363555 or http://dx.doi.org/10.2139/ssrn.3363555

[4] SAE International. (Jan. 2014). *Taxonomy and Definitions for Terms Related to On-Road Motor Vehicle Automated Driving Systems J3016_201401*. Accessed: Jan. 30, 2020. [Online]. Available: https://www.sae.org/standards/content/j3016_201401/preview/

[5] L. Hobert, A. Festag, I. Llatser, L. Altomare, F. Visintainer, and A. Kovacs, "Enhancements of V2X communication in support of cooperative autonomous driving," *IEEE Commun. Mag.*, vol. 53, no. 12, pp. 64–70, Dec. 2015.

[6] G. Naik, B. Choudhury, and J.-M. Park, "IEEE 802.11bd & 5G NR V2X: Evolution of radio access technologies for V2X communications," *IEEE Access*, vol. 7, pp. 70169–70184, 2019.

[7] K. Ganesan, P. B. Mallick, J. Löhr, D. Karampatsis, and A. Kunz, "5G V2X architecture and radio aspects," in *Proc. IEEE Conf. Standards Commun. Netw. (CSCN)*, Oct. 2019, pp. 1–6.

[8] *Study on Enhancement of 3GPP Support for 5G V2X Services (V16.2.0, Release 16)*, document 3GPP TR 22.886, 3GPP, Dec. 2018.

[9] H. S. Ma, E. Zhang, S. Li, Z. Lv, and J. Hu, "A V2X design for 5G network based on requirements of autonomous driving," SAE Tech. Paper 2016-01-1887, 2016.

[10] K. Serizawa, M. Mikami, K. Moto, and H. Yoshino, "Field trial activities on 5G NR V2 V direct communication towards application to truck platooning," in *Proc. IEEE 90th Veh. Technol. Conf. (VTC-Fall)*, Sep. 2019, pp. 1–5.

[11] M. Gharba, H. Cao, S. Gangakhedkar, J. Eichinger, A. R. Ali, K. Ganesan, V. Jain, S. Lapoehn, T. Frankiewicz, T. Hesse, Y. Zou, C. Tang, and L. Gu, "5G enabled cooperative collision avoidance: System design and field test," in *Proc. IEEE 18th Int. Symp. A World Wireless, Mobile Multimedia Netw. (WoWMoM)*, Jun. 2017, pp. 1–6.

[12] J. Park, S. Samarakoon, H. Shiri, M. K. Abdel-Aziz, T. Nishio, A. Elgabli, and M. Bennis, "Extreme URLLC: Vision, challenges, and key enablers," 2020, *arXiv:2001.09683*. [Online]. Available: http://arxiv.org/abs/2001.09683

[13] W. Tong, A. Hussain, W. X. Bo, and S. Maharjan, "Artificial intelligence for vehicle-to-everything: A survey," *IEEE Access*, vol. 7, pp. 10823–10843, 2019.

[14] L. Nie, Y. Li, and X. Kong, "Spatio-temporal network traffic estimation and anomaly detection based on convolutional neural network in vehicular ad-hoc networks," *IEEE Access*, vol. 6, pp. 40168–40176, 2018.

[15] C. An and C. Wu, "Traffic big data assisted V2X communications toward smart transportation," *Wireless Netw.*, vol. 26, no. 3, pp. 1601–1610, Apr. 2020.

[16] W. Liu and Y. Shoji, "Edge-assisted vehicle mobility prediction to support V2X communications," *IEEE Trans. Veh. Technol.*, vol. 68, no. 10, pp. 10227–10238, Oct. 2019.

[17] J. Gao, M. R. A. Khandaker, F. Tariq, K.-K. Wong, and R. T. Khan, "Deep neural network based resource allocation for V2X communications," in *Proc. IEEE 90th Veh. Technol. Conf. (VTC-Fall)*, Sep. 2019, pp. 1–5.

[18] J. Toutouh and E. Alba, "A swarm algorithm for collaborative traffic in vehicular networks," *Veh. Commun.*, vol. 12, pp. 127–137, Apr. 2018.

[19] R. Zhang, X. Jiang, and R. Li, "Improved decomposition-based multi-objective cuckoo search algorithm for spectrum allocation in cognitive vehicular network," *Phys. Commun.*, vol. 34, pp. 301–309, Jun. 2019.

[20] B. Ramakrishnan, S. R. Sreedivya, and M. Selvi, "Adaptive routing protocol based on cuckoo search algorithm (ARP-CS) for secured vehicular ad hoc network (VANET)," *Int. J. Comput. Netw. Appl.*, vol. 2, no. 4, pp. 173–178, 2015.
[21] A. Malathi and N. Sreenath, "An efficient clustering algorithm for Vanet," *Int. J. Appl. Eng. Res.*, vol. 12, no. 9, pp. 2000–2005, 2017.
[22] J. Zhang, Y. Zheng, and D. Qi, "Deep spatio-temporal residual networks for citywide crowd flows prediction," in *Proc. 31st AAAI Conf. Artif. Intell.*, North America, Feb. 2017. Accessed: Mar. 18, 2020. [Online]. Available: https://www.aaai.org/ocs/index.php/AAAI/AAAI17/paper/view/14501/13964
[23] X. S. He, F. Wang, Y. Wang, and X.-S. Yang, "Global convergence analysis of cuckoo search using Markov theory," in *Nature-Inspired Algorithms and Applied Optimization*. Cham, Switzerland: Springer, 2018, pp. 53–67.
[24] X.-S. Yang and S. Deb, "Cuckoo search: Recent advances and applications," *Neural Comput. Appl.*, vol. 24, no. 1, pp. 169–174, Jan. 2014.
[25] M. Mareli and B. Twala, "An adaptive cuckoo search algorithm for optimisation," *Appl. Comput. Informat.*, vol. 14, no. 2, pp. 107–115, Jul. 2018.
[26] S. Rahnamaei Yahiabadi, B. Barekatain, and K. Raahemifar, "TIHOO: An enhanced hybrid routing protocol in vehicular ad-hoc networks," *EURASIP J. Wireless Commun. Netw.*, vol. 2019, no. 1, p. 192, Dec. 2019.
[27] A. Kout, S. Labed, S. Chikhi, and E. B. Bourennane, "AODVCS, a new bio-inspired routing protocol based on cuckoo search algorithm for mobile ad hoc networks," *Wireless Netw.*, vol. 24, no. 7, pp. 2509–2519, Oct. 2018.
[28] S. K. Erskine and K. M. Elleithy, "Secure intelligent vehicular network using fog computing," *Electronics*, vol. 8, no. 4, p. 455, 2019.
[29] R. Purkait and S. Tripathi, "Network condition and application-based data adaptive intelligent message routing in vehicular network," *Int. J. Commun. Syst.*, vol. 31, no. 4, p. e3483, 2018.
[30] J. Agrawal, A. Singhal, and R. N. Yadav, "Multipath routing in mobile ad-hoc network using meta-heuristic approach," in *Proc. Int. Conf. Adv. Comput., Commun. Informat. (ICACCI)*, Sep. 2017, pp. 1399–1406.
[31] J. C. Sekhar and R. S. Prasad, "Trust predicated routing framework with optimized cluster head selection using cuckoo search algorithm for MANET," *IEIE Trans. Smart Process. Comput.*, vol. 4, no. 2, pp. 115–125, 2015.
[32] R. Li and L. Jin, "Improved cuckoo algorithm for spectrum allocation in cognitive vehicular network," in *Proc. 5th Int. Conf. Syst. Informat. (ICSAI)*, Nov. 2018, pp. 828–833.
[33] R. Zhang, X. Jiang, and R. Li, "Decomposition based multiobjective spectrum allocation algorithm for cognitive vehicular networks," in *Proc. IEEE 17th Int. Conf. Commun. Technol. (ICCT)*, Oct. 2017, pp. 831–836.
[34] Z. Xin, D. Zhang, and Z. Chen, "Spectrum allocation of cognitive radio network based on improved cuckoo search algorithm," in *Proc. 2nd Int. Conf. Comput. Sci. Softw. Eng. (CSSE)*, 2019, pp. 18–23.
[35] A. Malviya and S. Nema, "Spectrum sensing in cognitive radio by advanced cuckoo search," *ASIAN J. Converg. Technol.*, vol. 5, no. 1, pp. 1–4, 2019.
[36] S. Mirjalili, S. M. Mirjalili, and A. Lewis, "Grey wolf optimizer," *Adv. Eng. Softw.*, vol. 69, pp. 46–61, Mar. 2014.
[37] J.-S. Wang, S.-X. Li, and J.-D. Song, "Cuckoo search algorithm based on repeat-cycle asymptotic self-learning and self-evolving disturbance for function optimization," *Comput. Intell. Neurosci.*, vol. 2015, Aug. 2015, Art. no. 374873.
[38] D. P. Kingma and J. Ba, "Adam: A method for stochastic optimization," 2014, *arXiv:1412.6980*. [Online]. Available: http://arxiv.org/abs/1412.6980
[39] H.-S. Ma, S.-X. Li, S.-F. Li, Z.-N. Lv, and J.-S. Wang, "An improved dynamic self-adaption cuckoo search algorithm based on collaboration between subpopulations," *Neural Comput. Appl.*, vol. 31, no. 5, pp. 1375–1389, May 2019.
[40] K. J. Berry, J. E. Johnston, P. W. Mielke, and L. A. Johnston, "Permutation methods. Part II," *WIREs Comput. Statist.*, vol. 10, no. 3, p. e1429, May 2018.

HUISHENG MA (Member, IEEE) received the Master of Engineering degree in communication and information system from Xidian University, in 2009. He is currently pursuing the Ph.D. degree in communication and information system with the Beijing University of Posts and Telecommunications, Beijing, China. His research interests include radio resource allocation for broadband wireless networks, system design for V2X, the IoT, and artificial intelligence algorithms.

SHUFANG LI (Senior Member, IEEE) received the Ph.D. degree from the Department of Electrical Engineering, Tsinghua University, China, in 1997. She is currently a Professor and a Ph.D. Adviser with the School of Information and Communication Engineering, Beijing University of Posts and Communications, China. She has published hundreds of technical articles interiorly and overseas, as well as several textbooks, translation works, and patents. Her research interests include EMI/EMC, cognitive radio networks, mobile communication test systems, simulation technology for electromagnetic environments and countermeasures for interference control, and so on.

ERQING ZHANG received the Ph.D. degree from the Department of Information and Communication Engineering, Beijing University of Posts and Telecommunications (BUPT), China, in 2014. From July 2014 to November 2016, she worked as a Postdoctoral Fellow with the Department of Electronic Engineering, Tsinghua University. She is currently a Research Assistant with BUPT, China. Her research interests include V2X, energy-efficient wireless communications, resource allocation, and cross-layer optimization for wireless networks.

ZHENGNAN LV received the Master of Engineering degree in communication and information system from Jilin University, in 2006. Since 2006, he has been a Communication Algorithm Engineer and a Technology Manager with Potevio Information Technology Company Ltd. His research interests include radio resource allocation for broadband wireless networks, V2X, the IoT, and artificial intelligence. He presided over and participated in several projects in the field of wireless communication supported by the National Science and Technology Major Project of China.

JING HU received the Master of Engineering degree in signal and information processing from Xidian University, in 2006. Since 2006, she has been a Communication Algorithm Engineer and the Technology Manager of Potevio Information Technology Company Ltd. Her research interests include radio resource allocation for broadband wireless networks, system design for V2X, and artificial intelligence.

XINLEI WEI received the M.A. degree in pattern recognition and intelligent systems from the Henan University of Technology, in 2012, and the Ph.D. degree in computer science and technology from the Beijing University of Posts and Telecommunications, in 2019. He is currently a Postdoctoral Research with the Research Institute of Highway Ministry of Transport. His research interests include cross-media information processing, computer vision and scene recognition, and artificial intelligence.